JGR Solid Earth

RESEARCH ARTICLE
10.1029/2021JB022399

Postseismic Deformation of the 2008 Wenchuan Earthquake Illuminates Lithospheric Rheological Structure and Dynamics of Eastern Tibet

Min Wang[1], Zheng-Kang Shen[2,3], Yan-Zhao Wang[1], Roland Bürgmann[4], Fan Wang[5], Pei-Zhen Zhang[6], Hua Liao[7], Rui Zhang[8], Qi Wang[9], Zai-Sen Jiang[10], Wei-Tao Chen[11], Ming Hao[12], Yu Li[8], Tie Gu[7], Wei Tao[1], Kang Wang[4], and Lian Xue[2]

[1]State Key Laboratory of Earthquake Dynamics, Institute of Geology, China Earthquake Administration, Beijing, China, [2]Department of Geophysics, School of Earth and Space Science, Peking University, Beijing, China, [3]Department of Earth, Planetary, and Space Sciences, University of California, Los Angeles, CA, USA, [4]Department of Earth and Planetary Science, University of California, Berkeley, CA, USA, [5]National Geomatics Center of China, Beijing, China, [6]Guangdong Provincial Key Laboratory of Geodynamics and Geohazards, School of Earth Sciences and Engineering, Sun Yat-Sen University, Guangzhou, China, [7]Sichuan Earthquake Administration, Chengdu, China, [8]China Earthquake Network Center, China Earthquake Administration, Beijing, China, [9]Centre of Space Research, China University of Geosciences, Wuhan, China, [10]Institute of Earthquake Science, China Earthquake Administration, Beijing, China, [11]Development Research Center, China Earthquake Administration, Beijing, China, [12]Second Monitoring and Application Center, China Earthquake Administration, Xi'an, China

Key Points:

- A comprehensive GPS data set is provided to cover nine years of three-dimensional (3D) postseismic displacements after the 2008 Wenchuan earthquake
- GPS constrained eastern Tibet Lithospheric rheological structure agrees with a "jelly sandwich" model, not models of much lower viscosities
- A conceptual 3D tectonic deformation model in eastern Tibet is proposed to characterize its dynamic deformation style and mechanisms

Supporting Information:

Supporting Information may be found in the online version of this article.

Correspondence to:

Z.-K. Shen and M. Wang,
zshen@ucla.edu;
wangmin@ies.ac.cn

Citation:

Wang, M., Shen, Z.-K., Wang, Y.-Z., Bürgmann, R., Wang, F., Zhang, P.-Z., et al. (2021). Postseismic deformation of the 2008 Wenchuan earthquake illuminates lithospheric rheological structure and dynamics of eastern Tibet. *Journal of Geophysical Research: Solid Earth*, *126*, e2021JB022399. https://doi.org/10.1029/2021JB022399

Received 8 MAY 2021
Accepted 6 AUG 2021

Abstract Tectonic research of the Tibetan Plateau has long focused on its deformation style and mechanisms. The 2008 Mw7.9 Wenchuan earthquake ruptured the Longmen Shan fault located at the eastern rim of the plateau and excited a viscoelastic response of the lithosphere. We infer a three-dimensional (3D) rheological structure of eastern Tibet from modeling nine years of postseismic displacements observed by GPS. Our solution provides tight constraints on the lower-crustal and upper-mantle steady-state viscosities of the Songpan-Ganzi Terrane as $(5.0 \pm 0.7) \times 10^{18}$ and $(1.3 \pm 0.3) \times 10^{19}$ Pa s, respectively, consistent with a "jelly sandwich" model of Tibet, but not with some crustal channel flow models featuring much lower viscosities. The inferred lower-crustal and upper-mantle transient viscosities are $(5.0 \pm 1.3) \times 10^{17}$ and $(5.0 \pm 1.5) \times 10^{18}$ Pa s, respectively, suggesting nonlinear deformation mechanisms. The adjacent West Qinling and Sichuan blocks feature an order-of-magnitude higher rheological strength, which is consistent with the changes in the crustal material properties and interseismic deformation style across the East Kunlun-Tazang and Longmen Shan faults. Our results enable us to propose a conceptual 3D tectonic deformation model, in which the eastward extrusion of Tibet is absorbed in the Songpan-Ganzi crust mainly by E-W shortening and N-S extension, accommodated through faulting of conjugate strike-slip faults in the upper crust and distributed shear in the lower crust.

Plain Language Summary One of the fundamental questions in Earth science is the deformation mechanism of the continents, which controls the topography of the land we live on, the distribution of the resources extracted to support our living, and the origins of natural hazards such as landslides and earthquakes. The Tibetan Plateau, arguably, is the best natural laboratory to study the deformation mechanism of the continents. In this study, we address two critically important and much debated problems in Tibetan Plateau dynamics; that is, the rheologic structure of the Tibetan lithosphere and how it deforms under tectonic loading. We use nine years of mostly unpublished three-dimensional (3D) deformation data collected in the aftermath of the 2008 Mw7.9 Wenchuan earthquake to infer the rheological structure of the eastern Tibet lithosphere. Our results are consistent with a "jelly sandwich" model, with a relatively weak lower crust underlain by a stronger upper mantle. However, they do not support the very low viscosities envisioned by some of the channel flow models of lower crustal deformation in eastern Tibet. We also propose a conceptual 3D tectonic deformation model, in which the eastward extrusion of Tibet is absorbed in the Songpan-Ganzi crust by E-W shortening and N-S extension, accommodated through conjugate faults in the upper crust and distributed shear in the lower crust.

1. Introduction

The tectonic deformation style of the Tibetan Plateau has been debated for decades, with a focus on whether it is fluid-like and spatially distributed or block-like and localized on major faults (e.g., Houseman & England, 1986; Tapponnier et al., 1982). Key to resolving this debate is the elucidating rheological structure of the plateau lithosphere, which determines how the underthrusting and indentation of the India plate into Tibet drive deformation in the crust and upper mantle across the wide collision zone. Different first-order rheological models have been proposed to interpret the dynamic deformation processes, such as the "jelly sandwich" model, assuming a relatively weak lower crust sandwiched between the mechanically stronger upper crust and lithospheric mantle, and the "crème brûlée" model, hypothesizing a strong and brittle upper crust underlain by a relatively weak substrate (Bürgmann & Dresen, 2008; Burov & Watts, 2006). One brand of the "sandwich" model, the "crustal channel flow" model (Clark & Royden, 2000; Cook & Royden, 2008) advocates a greatly weakened and mobile lower crust, whose flow thickens the Tibetan crust, leading to its collision with the Sichuan Basin crust and creating the Longmen Shan mountain range and thrust fault zone (e.g., Burchfiel et al., 2008). A contrasting model, however, based on balanced geologic cross-sections, argues that substantial crustal shortening across the eastern Tibet margin is accommodated by reverse faulting and folding, and there is no need to call on other uplift mechanisms across the Longmen Shan range (e.g., Hubbard & Shaw, 2009; Hubbard et al., 2010).

This debate has persisted for decades partly because of the lack of direct observational constraints. Seismic tomography, seismic reflection surveys, magnetotelluric imaging, heat flow measurements, and other geophysical observations can reveal the first-order structure of and ambient conditions in the lower crust and lithospheric mantle, but do not provide direct measurement of the rheological properties (e.g., Li et al., 2009; Liu et al., 2014; Rippe & Unsworth, 2010; Wang et al., 2013; Zhao et al., 2012). Rock rheology has been measured in lab experiments, but it is an open question whether results from lab observations can be appropriately scaled up to describe rheological behavior in the lithosphere (Bürgmann & Dresen, 2008; Thatcher & Pollitz, 2008). New approaches to probing rheological properties of the lithosphere have become available in recent years and have been applied to the Tibetan collision zone. For example, lake-loading related vertical deformation and longer-term shoreline deflections were used to constrain the rheology of the lower crust and upper mantle (e.g., Doin et al., 2015; Henriquet et al., 2019). Geodetic postseismic deformation measurements collected after large earthquakes were also used to constrain the rheological relaxation processes in the lower crust and upper mantle excited by large events within and surrounding the Tibetan Plateau, such as after the 2001 Mw7.8 Kokoxili, 2008 Mw7.9 Wenchuan, and 2015 Mw7.6 Gorkha earthquakes (e.g., Diao et al., 2018; Huang et al., 2014; P. C. He et al., 2018; Ryder et al., 2011; Zhao et al., 2017).

The Mw7.9 Wenchuan earthquake occurred on May 12, 2008 at the eastern margin of the Tibetan Plateau, western China, and ruptured the central section of the transpressional Longmen Shan fault (e.g., Xu et al., 2009) which separates the Sichuan Basin from the Songpan-Ganzi Terrane in eastern Tibet (Figure 1). A number of postseismic deformation studies following this quake were carried out to investigate the rheological structures of the Sichuan Basin and Songpan-Ganzi region constrained by GPS and/or InSAR data (Diao et al., 2018; Ding et al., 2013; Huang et al., 2014; Jiang et al., 2017; Shao et al., 2011; Xu et al., 2014). Their estimated viscosities for the Songpan-Ganzi lower crust ranged from 4×10^{17} Pa s to 2×10^{19} Pa s (Table 1). This wide range of viscosity estimates is the result of multiple factors, such as using only the early period of postseismic observations for model constraints or ignoring contributions from afterslip and/or an initial period of transient viscoelastic relaxation.

In this study we report a new GPS data set of 3D postseismic displacement field collected across eastern Tibet and the western Sichuan Basin after the Wenchuan earthquake. This data set includes 86 site time series and covers a wide spatial range of the deformation from near-, mid- to far-field, and spans a wide temporal spectrum from days to nine years after the quake. Using this data set, we model the deformation processes and invert for spatially and temporally variable rheological properties and afterslip. The modeling results are more detailed and robust than previous ones and support a conceptual 3D tectonic deformation model for the eastern Tibetan Plateau and the Longmen Shan orogen. The results also give rise to better understanding of mechanical coupling within the crust and stress/strain evolution through an earthquake cycle.

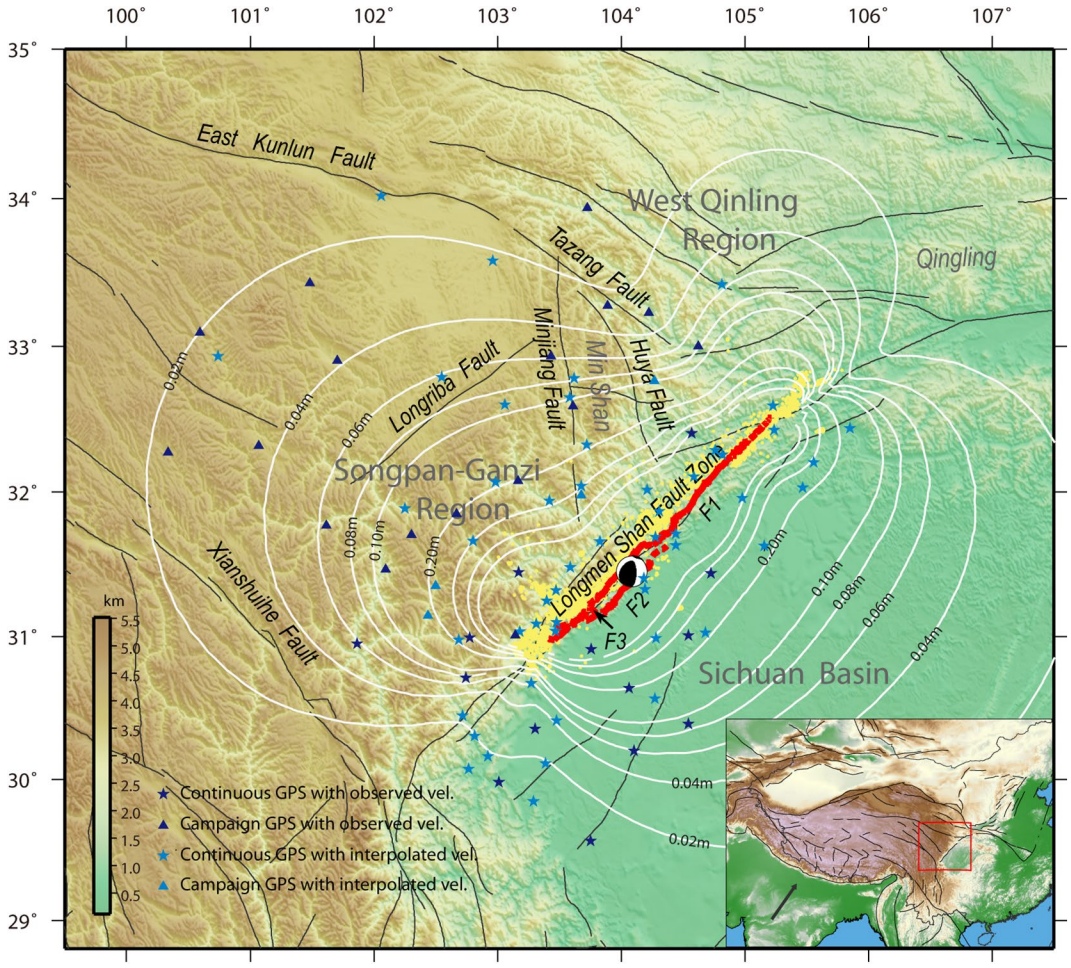

Figure 1. Tectonic setting of study area. The thick red lines indicate the surface rupture trace of the Wenchuan earthquake (Xu et al., 2009), and F1, F2, and F3 represent the Beichuan, Pengguan, and Xiaoyudong rupture branches, respectively. The white contours denote amplitudes of the total coseismic displacements derived from a coseismic slip model (Wan et al., 2017). The yellow dots denote $M \geq 2.0$ aftershocks that occurred within the first half-year and ~100 km of the rupture (Chen et al., 2009). The mainshock focal mechanism is from http://www.globalcmt.org/CMTcite.html (Ekström et al., 2012). Stars and triangles mark the locations of continuous and campaign GPS sites, respectively, with dark blue and light blue symbols representing sites with directly observed and interpolated pre-earthquake velocities, respectively.

2. GPS Data and Postseismic Displacement Time Series

The GPS data used in our study come from multiple sources, including: (a) Continuous sites installed after the earthquake by the China Earthquake Administration (CEA) and Peking University, which are located close to and at intermediate distances from the fault rupture. (b) Continuous sites in the Sichuan Province operated by the Sichuan Earthquake Administration, some of which were installed prior to the quake. (c) Campaign and continuous sites from the Crustal Motion Observation Network of China (CMONOC) project (Li et al., 2012), with 4–5 rounds of surveys within an 8-year time span before the quake for most of the campaign sites.

We use the GAMIT/GLOBK software package (Herring et al., 2010a, 2010b) to process the GPS data. The daily RINEX data from regional sites are processed together with data from regional CMONOC and IGS continuous sites, and the solutions are combined with the global solutions to realize the Terrestrial Reference Frame ITRF2008. More details about the data processing are described in Wang and Shen (2020). Then, the postseismic displacement time series of each site is derived by removing the secular motion using its preseismic secular velocity (Figure S1), which is obtained from either the preseismic observations at the

Table 1
Summary of Modeling Results of Wenchuan Postseismic Deformation

Reference	Data type	Number of GPS site	Data temporal coverage	Data spatial coverage	Mechanism	Range of AS (km)	Depth (km) & Viscosity (Pa s) for SGB	
Shao et al. (2011)	GPS	32	0–14 day	Near–mid field	AS + VR	0–40	25–60	MV = 4×10^{17}
Ding et al. (2013)	GPS	16	0–1 year	Near–mid field	VR	—	≥45	MV = 1.8×10^{19}
Huang et al. (2014)	GPS + InSAR	~30	0–1.5 years	Near–mid field	AS + VR	0–55	45–60	LV = 1.0×10^{18}
Xu et al. (2014)	GPS	10	0.5–5 years	Near–mid field	VR	—	25–60	MV ≥ 3.0×10^{18}
Jiang et al. (2017)	GPS	53	0–1 year	Near–far field	AS + VR[a]	0–160	45–60	LV = 1.0×10^{18}
Diao et al. (2018)	GPS	41	1.3–7 years	Near–far field	AS + VR	0–50	35–60	MV = 2.0×10^{18}
This study	GPS	86	0–9 years	Near–far field	AS + VR	0–70	≥30	

Abbreviations: AS, afterslip; LV, Burgers body steady-state viscosity; MV, Maxwell fluid viscosity; Range of AS, Downdip extent of AS along fault ramp; SGB, Songpan-Ganzi block; VR, viscoelastic relaxation.
[a]a priori value.

same location or an interpolation of preseismic velocities of surrounding sites (Wang & Shen, 2020) using the algorithm of Shen et al. (2015).

For the postseismic displacement time series of continuous sites, seasonal variations and jumps caused by the 2011 Mw9.0 Tohoku-Oki and 2013 Mw6.6 Lushan earthquakes are visible and removed by functional modeling of the time series (Text S1 and Figure S2; Z. Jiang, 2014; M. Wang et al., 2011). The Lushan earthquake occurred ~70 km southwest of the Wenchuan surface rupture, but no resolvable postseismic displacements associated with this event were observed at our sites. Seven pairs of closely located sites (<5.0 km in distance, see Figure S1) display consistent displacements during their overlapping observation periods, and their time series are merged. In all, a total of 86 site time series are included in this study, of which 80 consist of full 3D components and six have only their horizontal components used, respectively. These six sites had only half a year of measurements, resulting in large errors in their vertical components due to seasonal variations. The site locations and observation histories are shown in Figures 1 and S3, respectively.

Uncertainties of the displacement time series obtained as described above are formal error estimates, reflecting only internal errors of the data. For the campaign sites, the internal errors do not account for the effects of unstable benchmarks, setup errors of the instruments, and systematic deviations between different instruments, we therefore amplify the uncertainties of the displacement time series by a factor of two to account for these external errors. Furthermore, since the near-field GPS observations are sensitive to the changes of the fault geometry and slip distribution, which generally are not well represented in a smoothed fault slip model, we increase the data uncertainties by an ad hoc factor of $\left(1 + 3/\sqrt{D}\right)$, where D is the distance to the fault rupture at the surface in kilometer. Lastly, we take into account the effects of errors in preseismic secular velocities and add those uncertainties to the position errors of the postseismic displacement time series. The secular velocity uncertainties are estimated for their east, north, and up components as 0.2, 0.2, and 0.5 mm/yr for the continuous sites with four years of preseismic data, and 0.5, 0.5, and 1 mm/yr for the campaign sites with 8 years of preseismic data, respectively. We use 0.8, 0.8, and 1 mm/yr for the interpolated preseismic velocities.

3. Finite Element Model and Modeling Method

3.1. Finite Element Model

Geologic, geodetic, and geophysical imaging studies document a complex fault geometry and lithospheric structure of the Longmen Shan region (e.g., Burchfiel et al., 1995; Jia et al., 2014; Wan et al., 2017). We devise a finite element model (FEM) mesh to represent a first-order 3D structure of the Longmen Shan faults in a layered lithosphere, featuring a sharp contrast across the Longmen Shan fault, with the Moho at 42 km depth underneath the Sichuan Basin and 55 km depth underneath the Songpan-Ganzi block, respectively

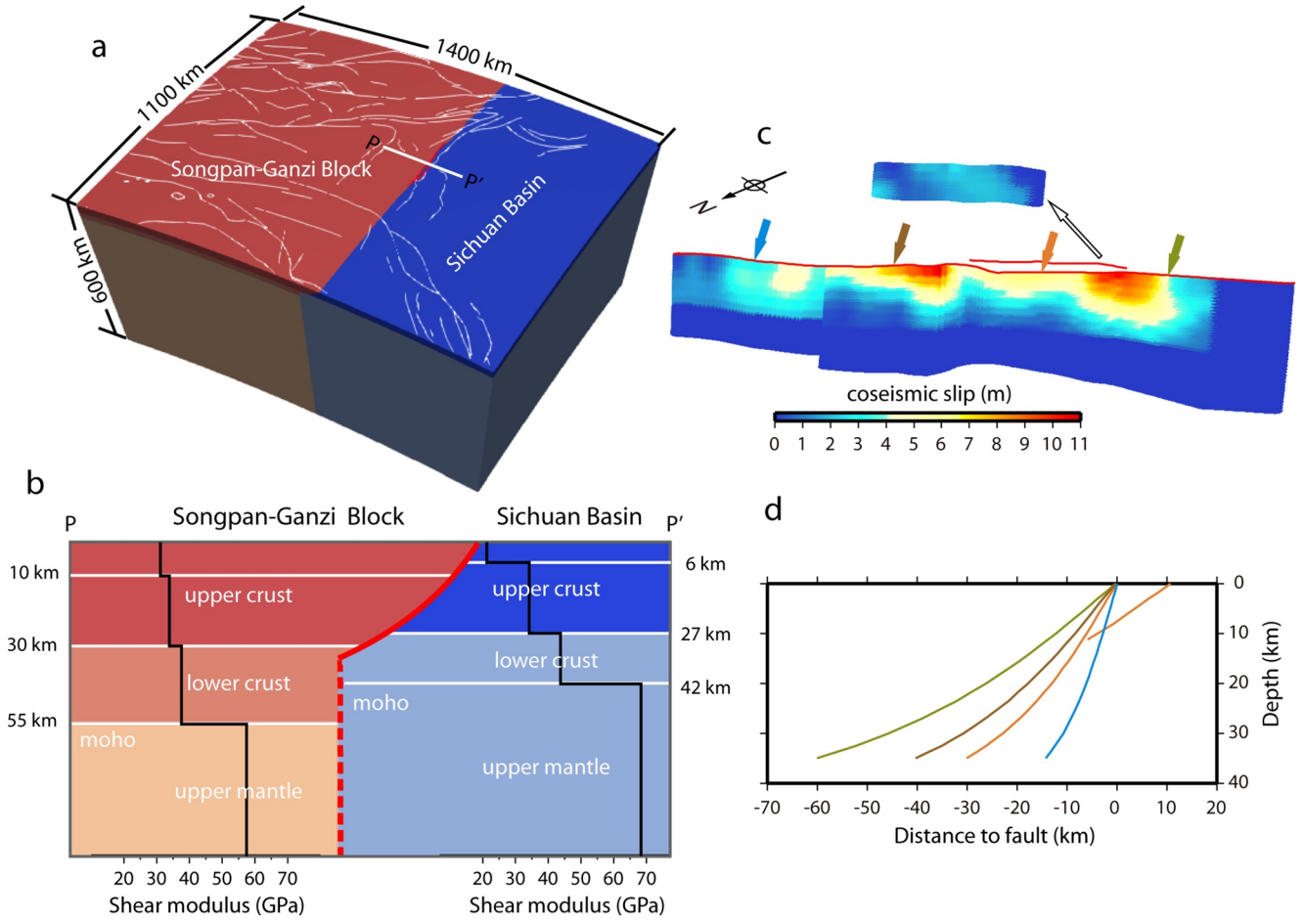

Figure 2. Three-dimensional finite element model configuration. (a) Model dimensions. (b) 2D model structure. The black curves denote the vertical profiles of shear modulus. The material domains of different viscosities are distinguished by colors. The white lines delineated layers of different elastic properties. (c) Fault geometry and slip distribution modified from Wan et al. (2017). (d) Vertical cross-sections of listric fault segments normal to surface trace. Locations of the profiles along the fault strike are marked in (c) as arrows with the corresponding colors.

(Figure 2). Elastic layered structures on either side of the fault are based primarily on seismic reflection and tomography results of Jia et al. (2014) and Xu et al. (2010). The FEM extends for 1,400 × 1,100 km in horizontal and 600 km in vertical directions, to sufficiently cover the extent of deformation caused by the Wenchuan earthquake and minimize any artifacts from using fixed boundary conditions.

The fault model, hosting the primary rupture of the Beichuan fault and the secondary rupture of the Pengguan fault, is modified from Wan et al. (2017), with minor adjustments of the geometry and coseismic slip distribution to match the FEM mesh. The Beichuan fault is listric in shape and dips to the NW, with the dip angle steepening from SW to NE. The fault plane is extended both laterally and downdip to 35 km depth to allow afterslip spread into the peripheral fault sections. The downdip extent along the fault ramp reaches up to 70 km from the surface trace. The coseismic displacements and stress field predicted by this modified model are in good agreement with that of Wan et al. (2017).

We invoke the Maxwell and Burgers materials to characterize viscoelastic relaxation processes of the Sichuan Basin substrate and Songpan-Ganzi block, respectively (see Text S2 for the rheological properties). For the Burgers body material of the Songpan-Ganzi block, we set the ratio of long-term to Maxwell shear modulus to 0.67, following Ryder et al. (2011). Two tests using different ratios show that this choice is reasonable (Text S2). We assume a uniform steady-state viscosity for the lower crust and upper mantle of the Sichuan Basin substrate. This is because the postseismic displacements at the Sichuan Basin sites are very

small and can be reasonably interpreted by the relatively simple rheological model, and more sophisticated rheological models would not improve the data fitting.

3.2. Modeling Method of Viscoelastic Relaxation and Afterslip

The observed postseismic deformation includes contributions from afterslip, poroelastic rebound, and viscoelastic relaxation of the lithosphere. We devise a joint inversion method to solve for the viscosities of the lithosphere media and afterslip distribution. The contribution due to poroelastic rebound is ignored, because it is concentrated only in the near field of the rupture and its effect is very small compared with the other two mechanisms (Diao et al., 2018; Huang et al., 2014). The inversion procedure follows a flowchart displayed in Figure S5. It starts with a panel of viscosity parameters and their possible variation ranges, and a grid-search within the ranges of the parameters is performed to determine the optimal solution of the viscosities. For a given set of viscosity values, we forward calculate the displacements caused by viscoelastic relaxation induced by coseismic stress changes, which are then differenced with the GPS observed time series to obtain the residuals time series to be used to constrain a fault afterslip model. Since afterslip generally occurs within a few months to a few years after the mainshock (Avouac, 2015), only the first four years of residual time series are used in the afterslip inversion.

We employ the finite element code PGCviscl-3D (Sun et al., 2017) to calculate surface displacements caused by both coseismic slip induced viscoelastic relaxation of the media and afterslip on fault. The optimal viscosity solution is obtained by grid-search seeking the minimum misfit defined as:

$$misfit = \frac{1}{n}\sum_{i=1}^{n}\lambda_i \times \chi_i^2 \tag{1}$$

where $\chi_i^2 = \frac{1}{m}\sum_{j=1}^{m}\left\{\sum_{k=1}^{3}\left[\left(d_o - d_p^r - d_p^a\right)^2/\sigma^2\right]_k\right\}_j$ is the mean sum of weighted displacement residual squares for the ith site time series, and m is the total number of epochs. d_o, d_p^r, d_p^a, and σ are the observed, model-predicted viscoelastic relaxation, model-predicted afterslip, and uncertainty of the kth component of the displacement at the jth epoch, respectively. $\lambda_i = s_i/\overline{s}$ is a reweighting factor, to balance the uneven distribution of geographic locations of sites (less weights are assigned for sites located in densely sampled regions), where s_i is the average distance between the ith site and its three nearest neighbors, and $\overline{s}$ is the average value of s_i for all the sites used in the modeling.

We adopt a logarithmic function to describe the time decay of postseismic displacements caused by afterslip on the Beichuan fault:

$$d_{res}(t) = d(t_0) + b\,ln\left(1 + \frac{t - t_0}{\tau}\right) \tag{2}$$

where $d_{\mathrm{res}}(t) = d_o(t) - d_p^r(t)$ is the data residual time series after subtraction of the model-predicted relaxation, $d(t_0)$ is the site position at the earthquake occurrence time t_0, and b and τ are the amplitude and decay time of the logarithmic function, respectively. Assuming that τ is a constant for all the sites, we use the residual time series from 18 near-field sites to solve for its optimal value, since the near-field observations are more sensitive to this parameter. After determination of the τ value, the amplitude b of the logarithmic decay function for each site is estimated using the least squares method.

In the afterslip inversion, we employ the least squares method with geometric smoothing of afterslip on fault, and minimize the following function

$$L(s) = \left\|D_B^{-1}(Gs - B)\right\|^2 + \frac{1}{\beta^2}\|Hs\|^2 \tag{3}$$

where s is a set of fault slip vectors with horizontal and updip components, G is the elastic Green's function matrix, B and D_B are the array of amplitude b and its variance matrix. H is the normal matrix for the first-order smoothing, and β is the smoothing factor determined by considering the trade-off between the parameter resolution and the data postfit residual chi-square. A non-negativity constraint is also imposed on fault slip; that is, only right-lateral and thrust motions are allowed.

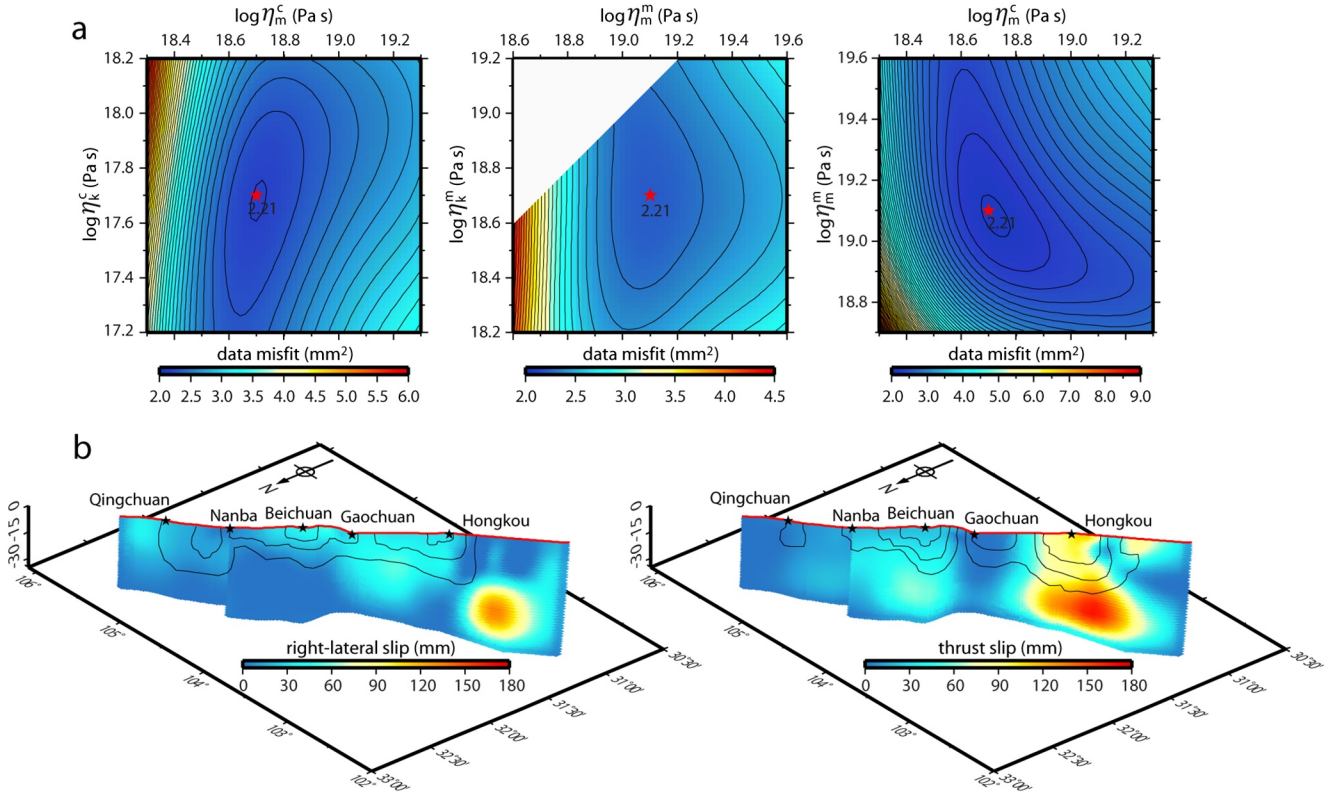

Figure 3. Results of preferred model with viscoelastic relaxation and afterslip. (a) Data misfit of joint model as function of viscosity parameter pairs of Songpan-Ganzi block. Left, central, and right panels are transient versus steady-state viscosity of lower crust, transient versus steady-state viscosity of upper mantle, and steady-state viscosity of lower crust versus steady-state viscosity of upper mantle, respectively, with other parameters fixed at their optimal values. The red stars mark the solution with minimum data misfit. The void area in the central panel denotes the part of parameter space with physically unreasonable parameters (transient viscosity > steady-state viscosity). (b) Afterslip result. Left and right panels are right-lateral and thrust components of the first year cumulative afterslip (with a decay time constant of 120 days), respectively, constrained with the optimal viscosity model and 20 mm spatial smoothing. The dark contours denote coseismic slips of 2, 4, and 6 m.

4. Rheology of Songpan-Ganzi Block and Afterslip Distribution on Fault

We use the displacement time series as constraints to solve for the kinematic afterslip distribution on the Beichuan fault (which approximates the gross effect of afterslip on the Beichuan and Pengguan faults) and the transient and steady-state viscosities of the lower crustal and upper mantle of the Songpan-Ganzi lithosphere. A simple Maxwell rheology model is invoked for the Sichuan Basin substrate material, whose steady-state viscosity is found to be $\geq 10^{20}$ Pa s (Text S3), which is consistent with the estimate of Huang et al. (2014). We therefore fix the steady-state viscosity of the Sichuan Basin substrate at 10^{20} Pa s in the subsequent modeling.

Using a grid-search approach described above, we determine the optimal viscosities of the lower-crustal transient (η_k^c), lower-crustal steady-state (η_m^c), upper-mantle transient (η_k^m), and upper-mantle steady-state (η_m^m) as $10^{17.7}$, $10^{18.7}$, $10^{18.7}$, and $10^{19.1}$ Pa s, respectively (Figure 3a), as well as the cumulative afterslip of the first year with a logarithmic decay time constant of 120 days (Figure 3b). The afterslip distribution is constrained by spatial smoothing with an optimal smoothing factor of 20 mm (Text S4). We call this model the preferred model to distinguish it from the later test models. The observed and model-predicted postseismic displacements are shown in Figure 4a, which demonstrates a good modeling fit of the data, particularly for the horizontal components. These data span different time periods (Figure S3), and the good fit to the cumulative displacements implies good agreement in the temporal evolution as well, which is confirmed by the fitting of displacement time series (Figure 4b and supporting information of GPS time series data).

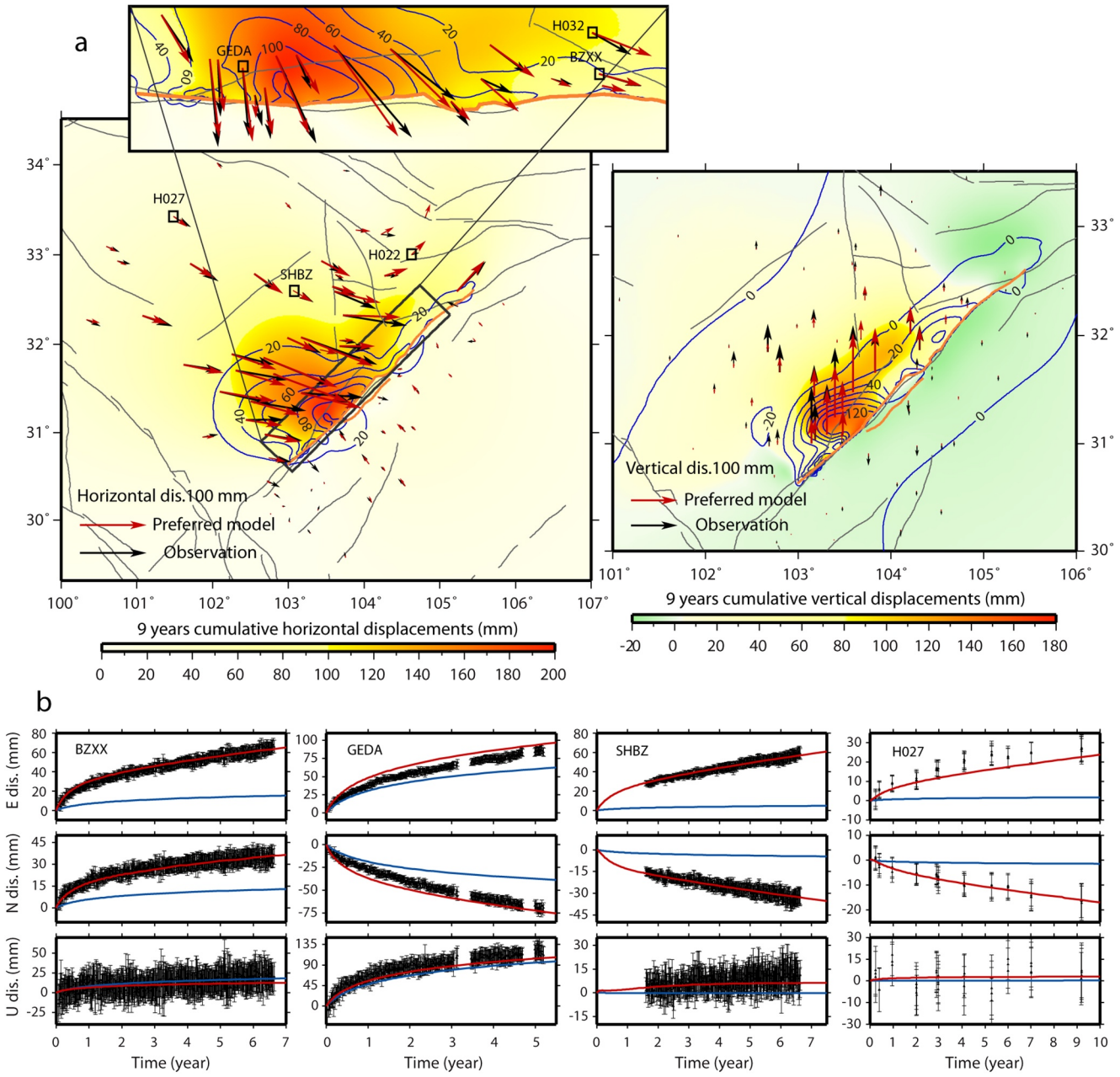

Figure 4. Data fitting of preferred model. (a) Left and right panels are horizontal and vertical components respectively. The solid orange lines mark the surface trace of the coseismic fault rupture. The black and red vectors represent the observed and model-predicted postseismic displacements in their respective observation periods. The background color represents nine years cumulative displacements after the quake predicted by the model, and the contours denote the contributions from afterslip only. (b) Time series fitting at 4 sites, whose locations are marked in (a). The blue and red curves are predicted contributions from afterslip only and viscoelastic relaxation plus afterslip, respectively.

Figure 3a shows data misfit as a function of viscosity parameter pairs of the Songpan-Ganzi block. The misfit is especially sensitive to the steady-state viscosities, which is reasonable since the deformation caused by steady-state relaxation has longer duration and was recorded better by the surveying network. Although the steady-state viscosities of the lower crust and upper mantle for the Songpan-Ganzi block are negatively correlated, they are still well constrained within a limited range. In contrast, the misfit is less sensitive to the transient viscosities. For the lower crust, this is partly because the surface displacements due to the transient relaxation have a similar temporal evolution pattern to that caused by afterslip, and the two processes

exhibit significant trade-off in the solution (Text S5). For the upper mantle, the poorer resolution of the transient viscosity is mainly due to the relatively weak signals in the far field.

The model results indicate early rapid postseismic deformation following the Wenchuan earthquake in the Songpan-Ganzi region, contributed by not only afterslip, but also stress-dependent transient relaxation of the lithosphere. This result suggests that the viscoelastic deformation is dominated by dislocation (power-law) creep in which the nominal viscosity increases as the driving stress relaxes with time (Bürgmann & Dresen, 2008). Our solution determines that the aseismic moment release due to the first 4 years of cumulative afterslip is 6.3×10^{19} Nm, which accounts for only ~7% of the coseismic moment release. This estimate is much smaller than that estimated by Diao et al. (2018), whose postseismic deformation model did not involve the transient relaxation process. Our results also show that because of the relatively minor contribution from afterslip, the effect of viscoelastic relaxation induced by afterslip can be neglected.

Our results also bring insight into the spatial and temporal evolution of the deformation field due to afterslip and viscoelastic relaxation (Figure 5). Both afterslip and viscoelastic relaxation contributed significantly to the near-to mid-field deformation. Most of the afterslip contribution concentrated in the vicinities of the Hongkou, Qingchuan, and Beichuan segments of the main rupture, and the viscoelastic relaxation affected a much broader region in the near- to middle-field on the hanging-wall side of the Longmen Shan fault zone, with larger contribution from relaxation of the lower crust than the upper mantle. The far-field postseismic deformation is moderate in amplitude but long lasting, with more contribution from relaxation of the upper mantle than the lower crust. For example, at a site ~300 km NW of the fault rupture, the apparent postseismic displacement rate is ~6.0 mm/yr one year after the quake, with ~3.8 mm/yr from the upper-mantle relaxation and ~2.2 mm/yr from the lower-crustal relaxation. By nine years after the quake, the rate is ~1.7 mm/yr, with ~1.1 mm/yr from the upper-mantle relaxation and ~0.6 mm/yr from the lower-crustal relaxation.

5. Discussion

5.1. Afterslip Model and Distribution

The kinematic afterslip distribution derived in the preferred model does not show a clear anti-correlation with the coseismic slip distribution in the seismogenic layer (Figure 3b). This result differs from one school of thought, which expects large afterslip to occur only in areas surrounding peak coseismic slip, where the Coulomb failure stress (CFS) is increased by the coseismic stress adjustment (e.g., Avouac, 2015; Bürgmann, 2018; Hsu et al., 2006). In previous studies of postseismic deformation, the coseismic CFS change was often used to constrain the afterslip distribution, such as Freed et al. (2006) for the 2002 Denali and Zhao et al. (2017) for the 2015 Gorkha earthquakes. As a test, we employ a similar method to Zhao et al. (2017) in the joint inversion to solve for stress-driven afterslip around the coseismic rupture (Text S6). This model produces a relatively poor data fitting, particularly for the near-field sites (Figure S9b), which is because the stress-driven afterslip model does not allow much shallow slip and constrains slip underneath the seismogenic layer to a narrow band (Figure S9a). Despite the difference in afterslip distribution, we find viscosity estimates of this model ($10^{17.7}$, $10^{18.8}$, $10^{18.6}$, and $10^{19.0}$ Pa s for η_k^c, η_m^c, η_k^m, and η_m^m) very close to those of the preferred model, confirming that the rheological properties of the Songpan-Ganzi block are robustly constrained by the mid- and far-field data, and not affected by different modeling approaches for afterslip.

The relatively poor data fitting of the test model with stress-driven afterslip suggests that the afterslip distribution is determined not only by coseismic CFS loading, but also by the rheological properties and geometry of the fault. Due to depth-dependent fault rheology (Blanpied et al., 1991), fault sections located deeper below the seismogenic layer may behave more "slip-strengthening" and are able to generate more aseismic slip after the quake. This means that the afterslip could be more broadly distributed in this depth range, as suggested by the kinematic afterslip model (Figure 3b). Extraordinarily large afterslip is found down-dip of the Hongkou segment, which could alternatively be explained by localized viscoelastic deformation in an anomalous seismic low-velocity zone (LVZ) detected by seismic tomography (Liu et al., 2014), and/or by fast creep on a ramp structure possibly extending into the middle crust underneath the Songpan-Ganzi Terrane (Li et al., 2010).

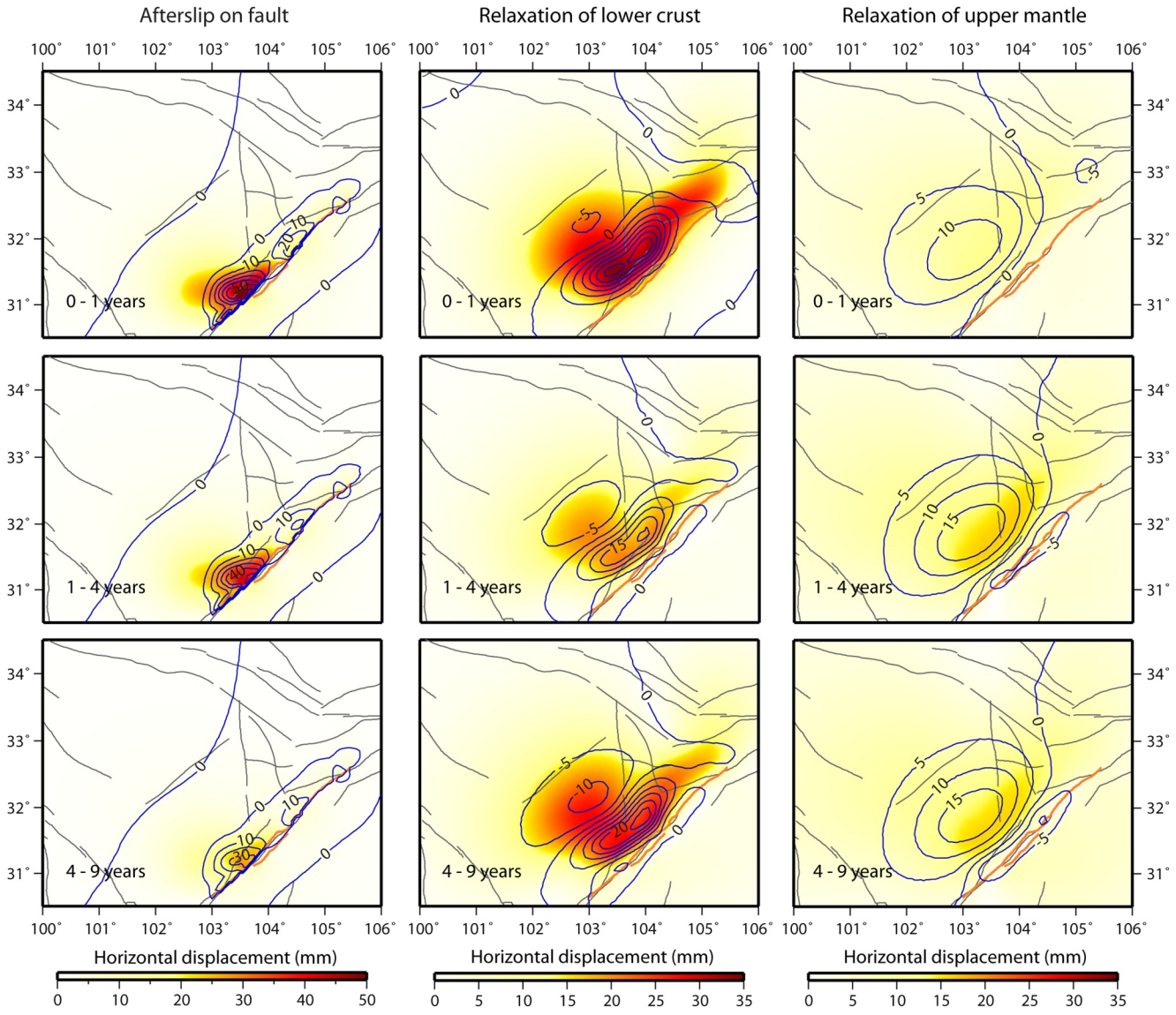

Figure 5. Cumulative displacement contributions of postseismic deformation processes. Left, central, and right panels show contributions from afterslip, viscoelastic relaxation of the Songpan-Ganzi lower crust, and relaxation of the Songpan-Ganzi upper mantle, respectively. The three rows show accumulated displacements at three different time periods. The background color and contours denote the amplitudes of the horizontal and vertical components, respectively.

Widespread shallow afterslip is also found in the kinematic afterslip model, with the largest values along the Hongkou segment. Shallow creep of the fault is supported by observations of repeating earthquakes (Li et al., 2011) and by observations from fault zone drilling, which showed a wide zone composed of highly fractured rocks saturated with water from the surface down to ~700 m depth (X. L. He et al., 2018). Besides, the Longmen Shan fault zone is composed of a series of geometric barriers (or irregularities), which largely controlled the coseismic slip distribution (Shen et al., 2009; Wan et al., 2017), and may have also controlled the afterslip distribution. The largest inferred afterslip in the seismogenic layer is located around the Xiaoyudong left step, which, although it experienced the maximum coseismic slip, may have also continued to slip postseismically to release residual stresses in a highly heterogeneous fault zone.

5.2. Role of Mid-Crustal Detachment Fault

Receiver function and seismic reflection studies have detected a negative impedance contrast interface and LVZ in the middle crust (20–40 km depth) underneath the Songpan-Ganzi region (Li et al., 2014; Wang et al., 2018; Yang et al., 2012). The inferred LVZ appears correlated with regions of high electrical conductivity (Rippe & Unsworth, 2010; Zhao et al., 2012). One interpretation of these geophysical features is the existence of a mid-crust detachment fault that links to the Longmen Shan fault ramp. Thompson et al. (2015) proposed that the detachment is at least partially locked interseismically for a ∼100 km stretch from the fault ramp to the Longriba fault, and ruptured during the Wenchuan earthquake and hosted postseismic afterslip (Fielding et al., 2013; Wang, Qiao, et al., 2011). Existence of such an extensive brittle detachment is under question, however, as seismic reflection studies (Guo et al., 2013; Wang et al., 2018) detected only fragmented reflectors in the middle crust with various vertical offsets, which may not support a continuous slip interface required by the detachment model. Also, most of the coseismic studies of the Wenchuan earthquake found no detectable slip on the fault ramp below ∼20 km depth or on a detachment far to the NW of the Longmen Shan (Feng et al., 2010; Tong et al., 2010). Other geodetic studies claimed patchy coseismic slip there (Wang, Qiao, et al., 2011), which, however, could be due to early localized afterslip, viscoelastic relaxation of weak zones in the middle crust, or errors caused by loose slip constraints in the inversion. A detachment fault below 20 km depth, if it existed, would likely be velocity strengthening (Blanpied et al., 1991), and more likely to slip aseismically than coseismically.

In our postseismic model we do not favor afterslip extending beyond ∼30 km northwest of the base of the mainshock rupture. Our model satisfactorily explains the mid- and far-field postseismic displacements with a rather limited number of rheological parameters, and we do not need to add far-reaching afterslip on a detachment to fit the data. In addition, widespread afterslip on a detachment would require a driving force, but the coseismically induced Coulomb stress changes are extremely low (<0.05 MPa) at mid-field distances (Toda et al., 2008) and would not be sufficient to induce significant afterslip there. Such a slip, even if it exists, would have to be on small patches of exceptionally weak faults with insignificant contributions to postseismic surface deformation.

5.3. Rheology of West Qinling Block

Although the preferred model explains the GPS data well in general, the data fitting result reveals a systematic deviation in the West Qinling region, with the predicted vectors moving a few tens of millimeters more northward than the observed (e.g., sites H022 and H032 in Figure 4a). A similar data misfit pattern was also reported by Huang et al. (2014). Seismic and magnetotelluric studies suggest a different crustal structure in this region from that of the Songpan-Ganzi region to the south. In particular, the lower crust of the Songpan-Ganzi region was found to have widespread zones with low seismic velocity and high electrical conductivity, which are largely absent in the West Qinling region (Li et al., 2014; Sun et al., 2018).

In order to investigate lithospheric rheology in the West Qinling region and its effect on the viscosity estimates of the Songpan-Ganzi block, we devise a test model, delineating the area north of the East Kunlun-Tazang fault and east of the Minjiang/Huya faults as a new "West Qinling" block, and allow the block to have its own rheological lithospheric structure. To reduce the dimension of the grid search, we fix the viscosities of the remaining Songpan-Ganzi block at the optimal values of the preferred model, and solve for viscosities of the West Qinling block and afterslip distribution. Since the number of GPS sites in the West Qinling block is too limited to resolve a layered structure, only the transient and steady-state viscosities for a combined layer of the lower crust and upper mantle are estimated. The preferred solution (Figure 6a) shows that the viscoelastic layer of the West Qinling block has a transient viscosity of $10^{18.5}$ Pa s and a steady-state viscosity close to or higher than 1×10^{20} Pa s. Both viscosities are significantly greater than that of the lower crust layer, and the steady-state viscosity is significantly greater than that of the upper mantle layer in the Songpan-Ganzi block, respectively.

Figure 6b illustrates that the test model improves the data fitting around the West Qinling region, with the data misfit reduced from 2.21 to 2.07 mm^2. Some systematic deviations persist, possibly due to complex geological structure in this region which cannot be represented by a simple model. The modeling result demonstrates that adjustment of viscosities of the West Qinling block only affects the deformation field in

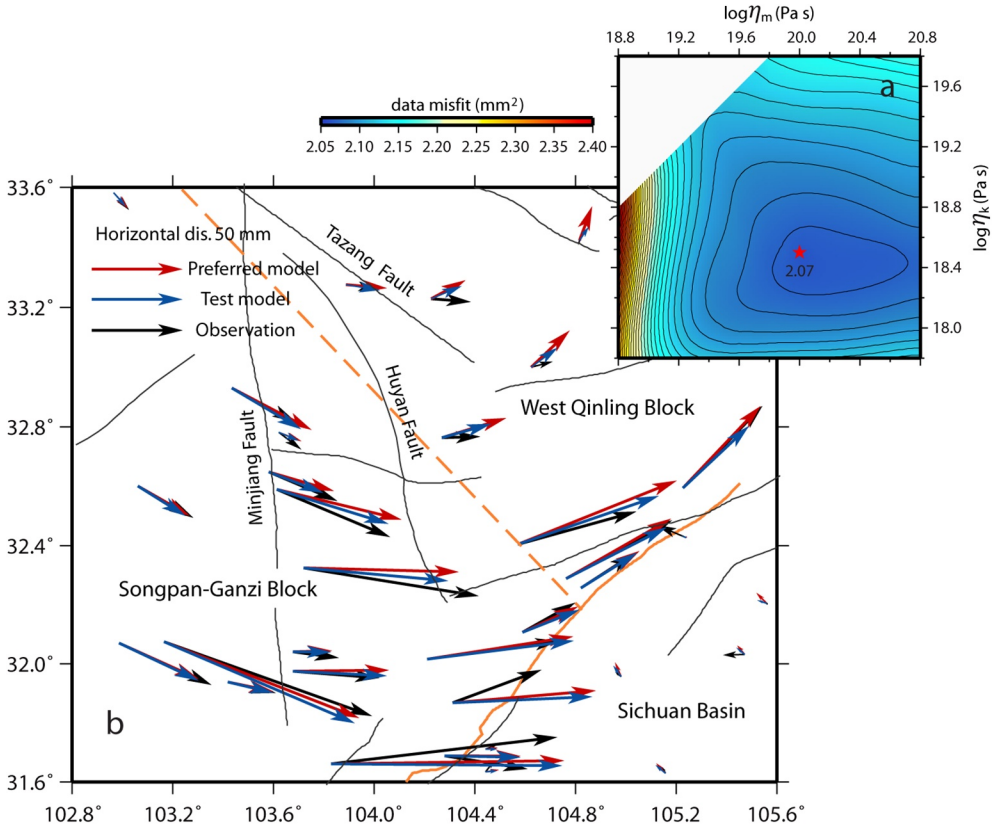

Figure 6. West Qinling block model and data fitting. (a) Data misfit as function of transient and steady-state viscosities of West Qinling block. Red star marks the selected solution. The void area denotes the part of parameter space with physically unreasonable parameters (transient viscosity > steady-state viscosity). (b) Comparison of model predicted GPS site cumulative displacements in their respective observation periods. Red and blue vectors are postseismic displacements predicted by the preferred model and the West Qinling test model, respectively. The solid and dashed orange lines mark the surface trace of the coseismic fault plane and the dividing line between the Songpan-Ganzi and West Qinling blocks, respectively.

its vicinity, not in the regions away from the West Qinling block. Therefore, the viscosity estimates of the Songpan-Ganzi block are not affected, since most GPS sites are far away from the West Qinling region.

The steady-state viscosity of the lower crust and upper mantle of the West Qinling block is close to or greater than 1×10^{20} Pa s, comparable to the Sichuan Basin. This suggests a mechanically stronger lower crust and upper mantle for the West Qinling block than for the adjoining Songpan-Ganzi block. This result is consistent with the findings of P. C. He et al. (2018), who used postseismic deformation data of the 2001 Mw 7.8 Kokoxili earthquake to study the lithospheric rheological structure around the East Kunlun fault. They estimated the steady-state viscosities of the combined lower crust and upper mantle substrate south and north of the East Kunlun fault as 1.5×10^{19} Pa s and 1.5×10^{20} Pa s, respectively, confirming the strong contrast in rheological properties across the East Kunlun-Tazang fault. The change in the interseismic deformation style across the East Kunlun-Tazang fault also supports a lateral contrast in the lithospheric rheological structure. The deformation field north of the fault can be modeled by block motion with little internal deformation (Loveless & Meade, 2011; Wang et al., 2017). This means that its deformation style is more block-like with brittle faulting at the block boundaries, suggesting that the crust is colder and more rigid in the West Qinling region. In contrast, smaller blocks with significant internal strain rates are needed to explain the deformation field south of the fault (Loveless & Meade, 2011; Wang et al., 2017), suggesting that the crust of the Songpan-Ganzi region is weaker, with the deformation accommodated by distributed shear, particularly in the middle to lower crust.

5.4. Lithospheric Rheological Structure in Eastern Tibet

The transient and steady-state viscosities of the upper mantle resolved by our model are both higher than those of the lower crust for the Songpan-Ganzi block, revealing a weak lower crust underlain by a relatively stronger upper mantle in this part of the plateau, consistent with the "jelly sandwich" model. This result is supported by other geophysical observations of the Songpan-Ganzi lithosphere, such as a thickened crust with widespread LVZs and low electrical-resistivity zones in the lower crust (Li et al., 2014; Liu et al., 2014; Rippe & Unsworth, 2010; Yang et al., 2012; Zhao et al., 2012), shallowly dipping seismic anisotropy in the lower crust (Xie et al., 2017), and relatively high heat flow measurements at the surface (Tao & Shen, 2008). All the evidence suggests hot and ductile materials, possibly with water and partial melt, in the lower crust of eastern Tibet.

Although our results confirm a "jelly sandwich" rheological structure in the Songpan-Ganzi region, it is still an open question whether the rheological structure would be consistent with one required by the crustal channel flow models (e.g., Clark & Royden, 2000; Cook & Royden, 2008). The lower-crustal flow models propose that the eastward extrusion of the Tibetan Plateau injects materials into the lower crust, which flows eastward with respect to the upper crust and mantle and creates the Longmen Shan orogen. To maintain the channel flow in these models, a very low viscosity ($\sim 10^{16}$–10^{17} Pa s) is required for the lower crust, which is about two orders of magnitude lower than our estimated value of $\sim 10^{18.7}$ Pa s. There might be some room for parameter adjustments to sustain the crustal flow in these models. For example, Cook and Royden (2008) opted for a channel 15 km thick with its viscosity $\eta = 10^{17}$ Pa s, and proposed that the channel flow could be sustained when $\eta \propto D^3$ (D is the thickness of the channel). Following this relation, if D increased to 30 km, η would rise up to $\sim 10^{17.9}$ Pa s, which nevertheless is still much lower than our estimate of $10^{18.7}$ Pa s. We conclude that although some form of "channel" may exist in this part of the crust, it may not be as weak and rapidly flowing as these channel flow models have envisioned.

5.5. Dynamics of Eastern Tibet Deformation

Various conceptual models have been proposed to describe the tectonic deformation in eastern Tibet (e.g., Jiang,Yang, & Zheng, 2014; Clark & Royden, 2000; Cook & Royden, 2008; England & Molnar, 2005; Flesch et al., 2001; Hubbard et al., 2010; Li et al., 2014; Loveless & Meade, 2011; Wang et al., 2017). These models provide interpretations based mostly on observations at the Earth's surface but differ markedly in the inferred mechanisms and deformation processes within the lithosphere. The key to constraining the deformation processes lies in the elucidating lithospheric structure, especially the rheological properties of the lower crust and upper mantle. Based on the rheological structure we obtained in this study and information from other geodetic, geophysical, and geologic studies, we propose a new conceptual tectonic deformation model for eastern Tibet, as illustrated in Figure 7.

Different from many of the previous studies, our model describes a 3D rheological structure and deformation pattern instead of 2D. To illustrate the deformation pattern in the Songpan-Ganzi Terrane, we analyze 1999–2007 GPS data and derive the 3D interseismic velocity field and horizontal strain-rate field before the Wenchuan earthquake (Figure 8). The geodetic strain-rate map reveals the horizontal principal strain rates of roughly E-W contraction and N-S extension at rates of 25–35 $\times 10^{-9}$/yr for most of the region, with contraction rates slightly higher than the extension rates. Such a strain-rate pattern is consistent with the faulting style of large-scale, conjugate strike-slip faults in the region, with sinistral shear across the NW trending Xianshuihe, WNW trending East Kunlun-Tazang, and NNW trending Huya faults (Sun et al., 2018), and dextral shear across the NE trending Longriba and oblique-reverse Beichuan (Xu et al., 2009) faults, respectively (Figure 7). In particular, the Longriba fault with shear motion of 4–6 mm/yr (Ren et al., 2013; Shen et al., 2005) results in northward bending of the East Kunlun-Tazang fault at the fault intersection, transferring part of the E-W shortening into N-S extension within the upper crust.

In addition to the elastic strain build-up around faults, the strain-rate field is also found to be broadly distributed (Wang et al., 2017), suggesting that the deformation field is at least partially coupled with and dictated by a mechanically weakened lower crust. Our model features a thickened lower crust with a steady-state viscosity of $10^{18.7}$ Pa s, which is weak enough to cause broadly distributed ductile deformation, and yet

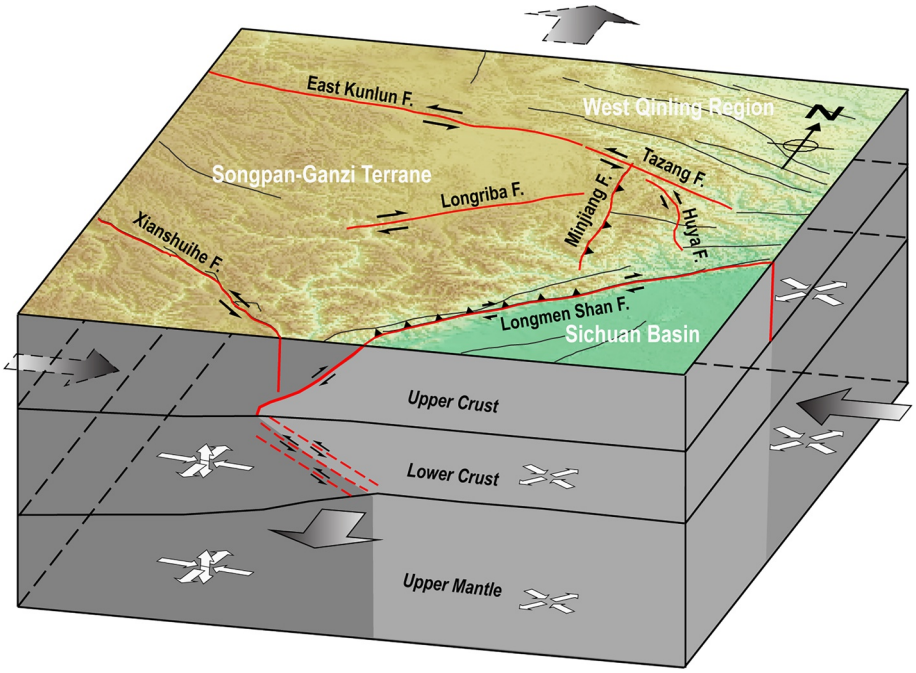

Figure 7. Three-dimensional tectonic deformation model of eastern Tibet. Solid red lines are major faults in the region, and black arrow pairs on fault indicate their sense of slip directions. Red dashed lines are inferred block boundaries in the lower crust. Large gray arrows denote displacement boundary conditions imposed by regional tectonics in the distributed collision zone, and the open orthogonal arrow pairs represent the 3D strain pattern in the lower crust and upper mantle.

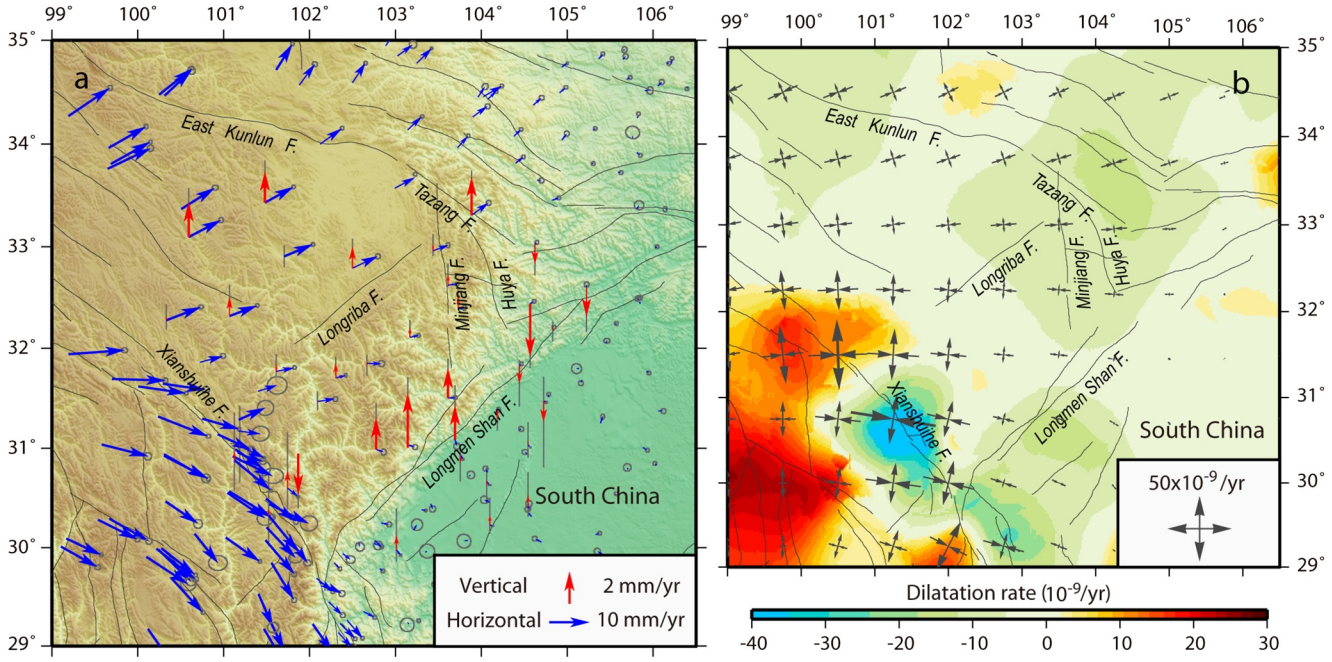

Figure 8. Geodetic deformation field before the Wenchuan earthquake in Songpan-Ganzi region and its vicinity. (a) GPS velocity field with respect to south China. (b) Horizontal dilatation rate (background color) and principal strain rates (arrow pairs) derived from the GPS velocities.

strong enough to facilitate interseismic coupling between the lower and upper crust and transmit at least part of the continuum deformation up to the surface.

The 3D deformation result shows that lateral shear is as important as or even more important than vertical thickening to accommodate E-W shortening in eastern Tibet. An average uplift rate of ~1 mm/yr for the interior of the Songpan-Ganzi region (Figure 8a), which is lower than that found in some previous studies (e.g., ~2.7 mm/yr uplift by Liang et al., 2013), yields a vertical extension rate of ~10–20 $\times$ 10^{-9}/yr within the lithosphere assuming a uniform strain to 50–100 km depth. Comparing with the horizontal strain rates of ~20–50 $\times$ 10^{-9}/yr for E-W shortening and ~10–30 $\times$ 10^{-9}/yr for N-S extension, we find that a modest amount of crustal thickening is balanced by the 2D horizontal areal reduction across the Songpan-Ganzi Terrane.

Seismic reflection and tomography studies discovered multiple reflectors dipping southeast in the lower crust underneath the Longmen Shan range (Feng et al., 2016; Guo et al., 2013), and abrupt thickening of the crust across the Sichuan Basin/Songpan-Ganzi Terrane boundary (Jia et al., 2014; Xu et al., 2010). This suggests that crustal shortening in this part of the plateau margin is unlikely to be caused by the Sichuan Basin subducting underneath the Songpan-Ganzi Terrane all the way to the Longriba fault (Thompson et al., 2015), since that would result in gradual thickening of the crust across the Longmen Shan range. Magnetotelluric results demonstrate a low electrical resistivity zone in the middle to lower crust NW of the Longmen Shan range underneath the Songpan-Ganzi Terrane (Zhao et al., 2012), which also seems to contradict the prediction of Sichuan Basin subduction. Instead, our model envisions that the Sichuan Basin wedges into the Songpan-Ganzi crust, causing its upper-crustal material to thrust above and its lower-crustal material to plunge underneath the Sichuan Basin, respectively (Figure 7). Our model is also consistent with the lack of late Cenozoic foreland subsidence in the Sichuan Basin (Burchfiel et al., 2008).

6. Conclusions

1. Using postseismic deformation data as model constraints, we have estimated the steady-state viscosities for the lower crust and upper mantle of the Songpan-Ganzi region as (5.0 $\pm$ 0.7) $\times$ 10^{18} and (1.3 $\pm$ 0.3) $\times$ 10^{19} Pa s respectively. This result is consistent with the "jelly sandwich" but not the "crème brûlée" lithosphere model. The steady-state viscosity of the lower crust is significantly higher than that proposed by some of the lower-crustal flow models.
2. The transient viscosities for the lower-crust and upper-mantle of the Songpan-Ganzi region are estimated as (5.0 $\pm$ 1.3) $\times$ 10^{17} and (5.0 $\pm$ 1.5) $\times$ 10^{18} Pa s respectively, which are about one order of magnitude smaller than the corresponding steady-state viscosities. The significant non-linear viscoelastic relaxation suggests that the process is dominated by dislocation creep. The transient relaxation contributes significantly to the near-to mid-field deformation within the first few years after the quake, and ignoring its contribution would lead to higher estimate of afterslip on fault and/or lower estimate of steady-state viscosity of the lithosphere.
3. Due to depth-dependent fault rheology and complex fault geometry, the afterslip for the Wenchuan earthquake is broadly distributed below the seismogenic layer, but it does not extend further to the northwest more than 60 km from the fault surface trace. This result does not support large scale detachment faulting during and after the quake in middle crust.
4. Mechanical properties differ significantly between the Sichuan Basin, Songpan-Ganzi, and West Qinling lithosphere. Steady-state viscosities are estimated as ~5 $\times$ 10^{18} Pa s and ~1 $\times$ 10^{19} Pa s for the lower crust and upper mantle of the Songpan-Ganzi block, and ~1 $\times$ 10^{20} Pa s for the lower crust and upper mantle of the Sichuan Basin and West Qinling block, respectively. The West Qinling and Sichuan Basin blocks feature an order-of-magnitude higher viscous flow strength, which illustrates well the changes in the interseismic deformation style across the East Kunlun-Tazang and Longmen Shan faults.
5. A new conceptual model is proposed for tectonic deformation of eastern Tibet. In the model the eastward extrusion of Tibet is absorbed in the Songpan-Ganzi crust mainly by E-W shortening and N-S extension, accommodated through faulting of conjugate strike-slip faults in the upper crust and distributed shear in the lower crust. Instead of rapid lower-crustal flow actively pushing up the Longmen Shan orogen, the lower crust deforms passively in response to E-W compression and absorbs horizontal shortening with broadly distributed ductile shear and vertical thickening of the crust.

Data Availability Statement

GPS site postseismic displacement time series data along with their plots are accessible at the Harvard Dataverse website https://doi.org/10.7910/DVN/V5LIHG.

Acknowledgments
The authors are very grateful to the field survey crews from the China Earthquake Administration, the Sichuan Bureau of Surveying, Mapping and Geoinformation, and the Sichuan Provincial Meteorological Service, whose names are not listed as coauthors, for their dedicated works of GPS data collection, particularly under harsh and dangerous conditions during the earthquake response phase after the Wenchuan earthquake. The authors also thank Qingliang Wang, Weijun Gan, Genru Xiao, and Guohu Chen for the field survey support they provided. The authors acknowledge Peng Li, Li Ren, and Hongbo Shi from the GPS Data Center, China Earthquake Administration for their constant support of GPS data acquisition and archiving. The authors are grateful to Jianbao Sun and Yongge Wan for their contributions to the coseismic slip model and useful discussions. The authors thank Kelin Wang, Jiangheng He, and Yan Hu for providing the PGCviscl-3D software and the technical support. Thoughtful and constructive review comments provided by Judith Hubbard and an anonymous reviewer helped improve the manuscript. This project has been supported by the National Natural Science Foundation of China (41090294, 41474028, 41774008), State Key Laboratory of Earthquake Dynamics (LED2008A05), and National Science Foundation (EAR-0911762, EAR-1723284).

References

Avouac, J. P. (2015). From geodetic imaging of seismic and aseismic fault slip to dynamic modeling of the seismic cycle. *Annual Review of Earth and Planetary Sciences*, *43*, 233–271. https://doi.org/10.1146/annurev-earth-060614-105302

Blanpied, M. L., Lockner, D. A., & Byerlee, J. D. (1991). Fault stability inferred from granite sliding experiments at hydrothermal conditions. *Geophysical Research Letters*, *18*(4), 609–612. https://doi.org/10.1029/91GL00469

Burchfiel, B. C., Chen, Z., Liu, Y., & Royden, L. H. (1995). Tectonics of the Longmen Shan and adjacent regions, central China. *International Geology Review*, *37*(8), 661–735. https://doi.org/10.1080/00206819509465424

Burchfiel, B. C., Royden, L. H., van der Hilst, R. D., Hager, B. H., Chen, Z., King, R. W., et al. (2008). A geological and geophysical context for the Wenchuan earthquake of 12 May 2008, Sichuan, people's republic of China. *Geological Society of America Today*, *18*(7), 4–11. https://doi.org/10.1130/GSATG18A.1

Bürgmann, R. (2018). The geophysics, geology and mechanics of slow fault slip. *Earth and Planetary Science Letters*, *495*, 112–134. https://doi.org/10.1016/j.epsl.2018.04.062

Bürgmann, R., & Dresen, G. (2008). Rheology of the lower crust and upper mantle: Evidence from rock mechanics, geodesy and field observations. *Annual Review of Earth and Planetary Sciences*, *36*(1), 531–567. https://doi.org/10.1146/annurev.earth.36.031207.124326

Burov, E. B., & Watts, A. B. (2006). The long-term strength of continental lithosphere: "jelly sandwich" or "crème brûlée"? *Geological Society of America Today*, *16*(1), 4—10. https://doi.org/10.1130/1052-5173(2006)016<4:TLTSOC>2.0.CO;2

Chen, J. H., Liu, Q. Y., Li, S. C., Guo, B., Li, Y., Wang, J., & Qi, S. H. (2009). Seismotectonic study by relocation of the Wenehuan Ms 8.0 earthquake sequence (in Chinese with an English abstract). *Chinese Journal of Geophysics*, *52*(2), 390–397.

Clark, M. K., & Royden, L. H. (2000). Topographic ooze: Building the eastern margin of Tibet by lower crustal flow. *Geology*, *28*(8), 703–706. https://doi.org/10.1130/0091-7613(2000)28<703:TOBTEM>2.0.CO;2

Cook, K. L., & Royden, L. H. (2008). The role of crustal strength variations in shaping orogenic plateaus, with application to Tibet. *Journal of Geophysical Research*, *113*, B08407. https://doi.org/10.1029/2007JB005457

Diao, F., Wang, R., Wang, Y., Xiong, X., & Walter, T. R. (2018). Fault behavior and lower crustal rheology inferred from the first seven years of postseismic GPS data after the 2008 Wenchuan earthquake. *Earth and Planetary Science Letters*, *495*, 202–212. https://doi.org/10.1016/j.epsl.2018.05.020

Ding, K., Xu, C., & Wen, Y. (2013). Postseismic deformation associated with the 2008 Wenchuan earthquake by GPS data (in Chinese with an English abstract). *Geomatics and Information Science of Wuhan University*, *38*, 131–135.

Doin, M.-P., Twardzik, C., Ducret, G., Lasserre, C., Guillaso, S., & Sun, J. (2015). InSAR measurement of the deformation around Siling Co Lake: Inferences on the lower crust viscosity in Central Tibet. *Journal of Geophysical Research: Solid Earth*, *120*(7), 5290–5310. https://doi.org/10.1002/2014JB011768

Ekström, G., Nettles, M., & Dziewonski, A. M. (2012). The global CMT project 2004-2010: Centroid-moment tensors for 13,017 earthquakes. *Physics of the Earth and Planetary Interiors*, *200–201*, 1–9. https://doi.org/10.1016/j.pepi.2012.04.002

England, P., & Molnar, P. (2005). Late quaternary to decadal velocity fields in Asia. *Journal of Geophysical Research*, *110*, B12401. https://doi.org/10.1029/2004JB003541

Feng, G., Hetland, E. A., Ding, X., Li, Z., & Zhang, L. (2010). Coseismic fault slip of the 2008 Mw 7.9 Wenchuan earthquake estimated from InSAR and GPS measurements. *Geophysical Research Letters*, *37*(1), L01302. https://doi.org/10.1029/2009GL041213

Feng, S.-Y., Zhang, P.-Z., Liu, B.-J., Wang, M., Zhu, S.-B., Ran, Y.-K., et al. (2016). Deep crustal deformation of the Longmen Shan, eastern margin of the Tibetan Plateau, from seismic reflection and Finite Element modeling. *Journal of Geophysical Research: Solid Earth*, *121*(2), 767–787. https://doi.org/10.1002/2015JB012352

Fielding, E. J., Sladen, A., Li, Z., Avouac, J.-P., Burgmann, R., & Ryder, I. (2013). Kinematic fault slip evolution source models of the 2008 M7.9 Wenchuan earthquake in China from SAR interferometry, GPS and teleseismic analysis and implications for Longmen Shan tectonics. *Geophysical Journal International*, *194*(2), 1138–1166. https://doi.org/10.1093/gji/ggt155

Flesch, L. M., Haines, A. J., & Holt, W. E. (2001). Dynamics of the India-Eurasia collision zone. *Journal of Geophysical Research*, *106*(B8), 16435–16460. https://doi.org/10.1029/2001jb000208

Freed, A. M., Bürgmann, R., Calais, E., & Freymueller, J. (2006). Stress-dependent power-law flow in the upper mantle following the 2002 Denali, Alaska, earthquake. *Earth and Planetary Science Letters*, *252*(3–4), 481–489. https://doi.org/10.1016/j.epsl.2006.10.011

Guo, X., Gao, R., Keller, G. R., Xu, X., Wang, H., & Li, W. (2013). Imaging the crustal structure beneath the eastern Tibetan Plateau and implications for the uplift of the Longmen Shan range. *Earth and Planetary Science Letters*, *379*, 72–80. https://doi.org/10.1016/j.epsl.2013.08.005

Henriquet, M., Avouac, J.-P., & Bills, B. G. (2019). Crustal rheology of southern Tibet constrained from lake-induced viscoelastic deformation. *Earth and Planetary Science Letters*, *506*, 308–322. https://doi.org/10.1016/j.epsl.2018.11.014

He, P. C., Wang, M., Wang, Q., & Shen, Z.-K. (2018). Rheological structure of lithosphere in northern Tibet inferred from postseismic deformation modeling of the 2001 Mw 7.8 Kokoxili earthquake (in Chinese with an English abstract). *Chinese Journal of Geophysics*, *61*, 531–544. https://doi.org/10.6038/cjg2018L0189

Herring, T. A., King, R. W., & McClusky, S. C. (2010a). *GAMIT reference manual, global Kalman filter VLBI and GPS analysis program* (Release 10.4). Cambridge, MA: Massachusetts Institute of Technology.

Herring, T. A., King, R. W., & McClusky, S. C. (2010b). *GAMIT reference manual, GPS analysis at MIT* (Release 10.4). Cambridge, MA: Massachusetts Institute of Technology.

He, X. L., Li, H. B., Wang, H., Zhang, L., Xu, Z. Q., & Si, J. L. (2018). Creeping along the Guanxian-Anxian fault of the 2008 Mw 7.9 Wenchuan earthquake in the Longmen Shan, China. *Tectonics*, *37*(7), 2124–2141. https://doi.org/10.1029/2017TC004820

Houseman, G., & England, P. (1986). Finite strain calculations of continental deformation 1: Method and general results for convergent zones. *Journal of Geophysical Research*, *91*(B3), 3651–3663. https://doi.org/10.1029/JB091iB03p03651

Hsu, Y.-J., Simons, M., Avouac, J.-P., Galetzka, J., Sieh, K., Chlieh, M., et al. (2006). Frictional afterslip following the 2005 Nias–Simeulue earthquake, Sumatra. *Science*, *312*(5782), 1921–1926. https://doi.org/10.1126/science.1126960

Huang, M.-H., Bürgmann, R., & Freed, A. M. (2014). Probing the lithospheric rheology across the eastern margin of the Tibetan plateau. *Earth and Planetary Science Letters*, *396*, 88–96. https://doi.org/10.1016/j.epsl.2014.04.003

Hubbard, J., & Shaw, J. H. (2009). Uplift of the Longmen Shan and Tibetan plateau, and the 2008 Wenchuan (M = 7.9) earthquake. *Nature*, *458*, 194–197. https://doi.org/10.1038/nature07837

Hubbard, J., Shaw, J. H., & Klinger, Y. (2010). Structural setting of the 2008 Mw 7.9 Wenchuan, China, earthquake. *Bulletin of the Seismological Society of America*, *100*(5B), 2713–2735. https://doi.org/10.1785/0120090341

Jiang, C., Yang, Y., & Zheng, Y. (2014). Penetration of mid-crustal low velocity zone across the Kunlun Fault in the NE Tibetan Plateau revealed by ambient noise tomography. *Earth and Planetary Science Letters*, *406*, 81–92. https://doi.org/10.1016/j.epsl.2014.08.040

Jiang, Z., Wang, M., Wang, Y., Wu, Y., Che, S., Shen, Z. K., et al. (2014). GPS constrained coseismic source and slip distribution of the 2013 Mw6.6 Lushan, China, earthquake and its tectonic implications. *Geophysical Research Letters*, *41*, 407–413. https://doi.org/10.1002/2013GL058812

Jiang, Z., Yuan, L., Huang, D., Yang, Z., & Chen, W. (2017). Postseismic deformation associated with the 2008 Mw 7.9 Wenchuan earthquake, China: Constraining fault geometry and investigating a detailed spatial distribution of afterslip. *Journal of Geodynamics*, *112*, 12–21. https://doi.org/10.1016/j.jog.2017.09.001

Jia, S., Liu, B., Xu, Z., Liu, Z., Feng, S., Zhang, J., et al. (2014). The crustal structures of the central Longmenshan along and its margins as related to the seismotectonics of the 2008 Wenchuan earthquake. *Science China Earth Sciences*, *57*, 777–790. https://doi.org/10.1007/s11430-013-4744-9

Liang, S., Gan, W., Shen, C., Xiao, G., Liu, J., Chen, W., et al. (2013). Three-dimensional velocity field of present day crustal motion of the Tibetan Plateau derived from GPS measurements. *Journal of Geophysical Research: Solid Earth*, *118*(10), 5722–5732. https://doi.org/10.1002/2013JB010503

Li, H., Shen, Y., Huang, Z., Li, X., Gong, M., Shi, D., et al. (2014). The distribution of the mid-to-lower crustal low-velocity zone beneath the northeastern Tibetan Plateau revealed from ambient noise tomography. *Journal of Geophysical Research: Solid Earth*, *119*(3), 1954–1970. https://doi.org/10.1002/2013JB010374

Li, H., Su, W., Wang, C.-Y., & Huang, Z. (2009). Ambient noise rayleigh wave tomography in western Sichuan and eastern Tibet. *Earth and Planetary Science Letters*, *282*(1–4), 201–211. https://doi.org/10.1016/j.epsl.2009.03.021

Li, L., Chen, Q.-F., Niu, F., & Su, J. (2011). Deep slip rates along the Longmen Shan fault zone estimated from repeating microearthquakes. *Journal of Geophysical Research*, *116*(B9), B09310. https://doi.org/10.1029/2011JB008406

Li, Q., You, X., Yang, S., Du, R., Qiao, X., Zou, R., & Wang, Q. (2012). A precise velocity field of tectonic deformation in China as inferred from intensive GPS observations. *Science China Earth Sciences*, *55*(5), 695–698. https://doi.org/10.1007/s11430-012-4412-5

Liu, Q. Y., van der Hilst, R. D., Li, Y., Yao, H. J., Chen, J. H., Guo, B., et al. (2014). Eastward expansion of the Tibetan Plateau by crustal flow and strain partitioning across faults. *Nature Geoscience*, *7*, 361–365. https://doi.org/10.1038/NGEO2130

Li, Y., Jia, D., Shaw, J. H., Hubbard, J., Lin, A., Wang, M., et al. (2010). Structural interpretation of the coseismic faults of the Wenchuan earthquake: Three-dimensional modeling of the Longmen Shan fold-and-thrust belt. *Journal of Geophysical Research*, *115*(B4), B04317. https://doi.org/10.1029/2009JB006824

Loveless, J. P., & Meade, B. J. (2011). Partitioning of localized and diffuse deformation in the Tibetan Plateau from joint inversions of geologic and geodetic observations. *Earth and Planetary Science Letters*, *303*(1–2), 11–24. https://doi.org/10.1016/j.epsl.2010.12.014

Ren, J., Xu, X., Yeats, R. S., & Zhang, S. (2013). Latest quaternary paleoseismology and slip rates of the Longriba fault zone, eastern Tibet: Implications for fault behavior and strain partitioning. *Tectonics*, *32*(2), 216–238. https://doi.org/10.1002/tect.20029

Rippe, D., & Unsworth, M. (2010). Quantifying crustal flow in Tibet with magnetotelluric data. *Physics of the Earth and Planetary Interiors*, *179*(3–4), 107–121. https://doi.org/10.1016/j.pepi.2010.01.009

Ryder, I., Bürgmann, R., & Pollitz, F. (2011). Lower crustal relaxation beneath the Tibetan plateau and Qaidam basin following the 2001 Kokoxili earthquake. *Geophysical Journal International*, *187*, 613–630. https://doi.org/10.1111/j.1365-246X.2011.05179.x

Shao, Z., Wang, R., Wu, Y., & Zhang, L. (2011). Rapid afterslip and short-term viscoelastic relaxation following the 2008 Mw 7.9 Wenchuan earthquake. *Earthquake Science*, *24*, 163–175. https://doi.org/10.1007/s11589-010-0781-z

Shen, Z.-K., Lü, J., Wang, M., & Bürgmann, R. (2005). Contemporary crustal deformation around the southeast bordland of the Tibetan Plateau. *Journal of Geophysical Research*, *110*, B11409. https://doi.org/10.1029/2004JB003421

Shen, Z.-K., Sun, J., Zhang, P., Wan, Y., Wang, M., Bürgmann, R., et al. (2009). Slip maxima at fault junctions and rupturing of barriers during the 2008 Wenchuan earthquake. *Nature Geoscience*, *2*, 718–724. https://doi.org/10.1038/NGEO636

Shen, Z.-K., Wang, M., Zeng, Y., & Wang, F. (2015). Optimal interpolation of spatially discretized geodetic data. *Bulletin of the Seismological Society of America*, *105*(4), 2117–2127. https://doi.org/10.1785/0120140247

Sun, J., Yue, H., Shen, Z., Fang, L., Zhan, Y., & Sun, X. (2018). The 2017 Jiuzhaigou earthquake: A complicated event occurred in a young fault system. *Geophysical Research Letters*, *45*(5), 2230–2240. https://doi.org/10.1002/2017GL076421

Sun, T., Wang, K., Fujiwara, T., Kodaira, S., & He, J. (2017). Large fault slip peaking at trench in the 2011 Tohoku-oki earthquake. *Nature Communications*, *8*(1), 14044. https://doi.org/10.1038/ncomms14044

Tao, W., & Shen, Z. (2008). Heat flow distribution in Chinese continent and its adjacent areas. *Progress in Natural Science*, *18*(7), 843–849. https://doi.org/10.1016/j.pnsc.2008.01.018

Tapponnier, P., Peltzer, G., Le Dain, A. Y., Armijo, R., & Cobbold, P. (1982). Propagating extrusion tectonics in Asia: New insights from simple experiments with plasticine. *Geology*, *10*, 611–616. https://doi.org/10.1130/0091-7613(1982)10<611:PETIAN>2.0.CO;2

Thatcher, W., & Pollitz, F. F. (2008). Temporal evolution of continental lithospheric strength in actively deforming regions. *Geological Society of America Today*, *18*(4/5), 4–11. https://doi.org/10.1130/GSAT01804-5A.1

Thompson, T. B., Plesch, A., Shaw, J. H., & Meade, B. J. (2015). Rapid slip-deficit rates at the eastern margin of the Tibetan Plateau prior to the 2008 Mw 7.9 Wenchuan earthquake. *Geophysical Research Letters*, *42*, 1677–1684. https://doi.org/10.1002/2014GL062833

Toda, S., Lin, J., Meghraoui, M., & Stein, R. S. (2008). 12 May 2008 M = 7.9 Wenchuan, China, earthquake calculated to increase failure stress and seismicity rate on three major fault systems. *Geophysical Research Letters*, *35*, L17305. https://doi.org/10.1029/2008GL034903

Tong, X., Sandwell, D. T., & Fialko, Y. (2010). Coseismic slip model of the 2008 Wenchuan earthquake derived from joint inversion of interferometric synthetic aperture radar, GPS, and field data. *Journal of Geophysical Research*, *115*(B4), B04314. https://doi.org/10.1029/2009JB006625

Wang, C.-Y., Chen, W.-P., & Wang, L.-P. (2013). Temperature beneath Tibet. *Earth and Planetary Science Letters*, *375*, 326–337. https://doi.org/10.1016/j.epsl.2013.05.052

Wang, M., Li, Q., Wang, F., Zhang, R., Wang, Y., Shi, H., et al. (2011). Far-field coseismic displacements associated with the 2011 Tohoku-Oki earthquake in Japan observed by global positioning system. *Chinese Science Bulletin*, *56*(23), 2419–2424. https://doi.org/10.1007/s11434-011-4588-7

Wang, M., & Shen, Z.-K. (2020). Present-day crustal deformation of continental China derived from GPS and its tectonic implications. *Journal of Geophysical Research: Solid Earth*, *125*, e2019JB018774. https://doi.org/10.1029/2019JB018774

Wang, Q., Qiao, X., Lan, Q., Freymueller, J., Yang, S., Xu, C., et al. (2011). Rupture of deep faults in the 2008 Wenchuan earthquake and uplift of the Longmen Shan. *Nature Geoscience*, *4*, 634–640. https://doi.org/10.1038/NGEO1210

Wang, X., Chen, L., Ai, Y., Xu, T., Jiang, M., Ling, Y., & Gao, Y. (2018). Crustal structure and deformation beneath eastern and northeastern Tibet revealed by P-wave receiver functions. *Earth and Planetary Science Letters*, *497*, 69–79. https://doi.org/10.1016/j.epsl.2018.06.007

Wang, Y., Wang, M., & Shen, Z.-K. (2017). Block-like versus distributed crustal deformation around the northeastern Tibetan plateau. *Journal of Asian Earth Sciences*, *140*, 31–47. https://doi.org/10.1016/j.jseaes.2017.02.040

Wan, Y., Shen, Z.-K., Bürgmann, R., Sun, J., & Wang, M. (2017). Fault geometry and slip distribution of the 2008 Mw 7.9 Wenchuan, China earthquake, inferred from GPS and InSAR measurements. *Geophysical Journal International*, *208*, 748–766. https://doi.org/10.1093/gji/ggw421

Xie, J., Ritzwoller, M. H., Shen, W., & Wang, W. (2017). Crustal anisotropy across eastern Tibet and surroundings modeled as a depth-dependent tilted hexagonally symmetric medium. *Geophysical Journal International*, *209*, 466–491. https://doi.org/10.1093/gji/ggx004

Xu, C. J., Fan, Q. B., Wang, Q., Yang, S. M., & Jiang, G. Y. (2014). Potseismic deformation after the 2008 Wenchuan earthquake. *Survey Review*, *46*, 432–436. https://doi.org/10.1179/1752270614Y.0000000128

Xu, X., Wen, X., Yu, G., Chen, G., Klinger, Y., Hubbard, J., & Shaw, J. (2009). Coseismic reverse- and oblique-slip surface faulting generated by the 2008 Mw 7.9 Wenchuan earthquake, China. *Geology*, *37*(6), 515–518. https://doi.org/10.1130/G25462A.1

Xu, Y., Li, Z., Huang, R., & Xu, Y. (2010). Seismic structure of the Longmen Shan region from S-wave tomography and its relationship with the Wenchuan Ms 8.0 earthquake on 12 May 2008, southwestern China. *Geophysical Research Letters*, *37*(2), L02304. https://doi.org/10.1029/2009GL041835

Yang, Y., Ritzwoller, M. H., Zheng, Y., Shen, W., Levshin, A. L., & Xie, Z. (2012). A synoptic view of the distribution and connectivity of the mid-crustal low velocity zone beneath Tibet. *Journal of Geophysical Research*, *117*(B4), B04303. https://doi.org/10.1029/2011JB008810

Zhao, B., Bürgmann, R., Wang, D., Tan, K., Du, R., & Zhang, R. (2017). Dominant controls of downdip afterslip and viscous relaxation on the postseismic displacements following the Mw7.9 Gorkha, Nepal, earthquake. *Journal of Geophysical Research: Solid Earth*, *122*, 8376–8401. https://doi.org/10.1002/2017JB014366

Zhao, G., Unsworth, M. J., Zhan, Y., Wang, L., Chen, X., Jones, A. G., et al. (2012). Crustal structure and rheology of the Longmenshan and Wenchuan Mw 7.9 earthquake epicentral area from magnetotelluric data. *Geology*, *40*(12), 1139–1142. https://doi.org/10.1130/G33703.1